Turing Patterns, Spatial Bistability, and Front Interactions in the [ClO_2, I_2, I^-, $CH_2(COOH)_2$] Reaction

Damián E. Strier, Patrick De Kepper, and Jacques Boissonade

Centre de Recherche Paul Pascal, C.N.R.S. Bordeaux, Avenue Schweitzer, F-33600 Pessac, France

Received: August 26, 2004; In Final Form: December 7, 2004

Recent experiments by Szalai and De Kepper[1] performed in open spatial reactors have shown that the rich variety of dynamic properties of the chlorine dioxide−iodide−chlorite−iodine−malonic acid family of reactions is far from being exhausted: stable inhomogeneous patterns due to front interactions and transient labyrinthine structures are now added to the spatial bistability and Turing patterns as possible spatial behavior. The two latter phenomena, already observed in the chlorine dioxide−iodide (CDI) and the chlorine dioxide−iodide−malonic acid (CDIMA) reactions, respectively, were kept as limiting cases in the new setup. In this paper, we numerically analyze an extension of the most detailed available model of the CDI system (Lengyel et al.[2]) including a reaction between I_2 and MA that comes from the presence of the latter into the flow. The resulting nine-variable model is simulated in one and two dimensions, taking into account the proper constraints of the boundary-fed system. The nonequilibrium phase diagram closely follows the results of the experiments of ref 1. In particular, the model reproduces observations on spatial bistability, stationary front interactions, and Turing patterns. In addition, it predicts a new region of spatial bistability.

1. Introduction

Reactions of chlorite ClO_2^- or chlorine dioxide ClO_2 with iodide I^- and/or iodine I_2 in acidic medium with possible additions of malonic acid MA and complexing agents for polyiodide, such as starch or poly(vinyl alcohol) (PVA), constitute an important family (hereafter referred to as the CI family) that has been the subject of detailed studies during the past decades. The CI family includes the chlorite−iodide−malonic acid (CIMA) reaction,[3,4] the chlorine dioxide−iodide (CDI) reaction,[2] and the chlorine dioxide−iodine−malonic acid (CDIMA) variants. They belong to the relatively small group of chemical reactions that display a rich variety of temporal and spatial behavior and, at the same time, are fairly well understood at the chemical level.

The CIMA reaction exhibits transient oscillatory behavior when it is performed in batch conditions. It has been demonstrated by Lengyel, Rábai, and Epstein[5] that there is a subsystem, driven by the CDIMA reaction, which is responsible for the oscillations. The most remarkable property of the CIMA and CDIMA reactions refers, however, to the spatial behavior, as revealed in experiments performed in open gel reactors. In those setups, input chemical species are fed into a piece of hydrogel by diffusion from a boundary in contact with a continuously strirred tank reactor (CSTR). While the concentrations in the CSTR are kept at fixed and homogeneous values, stationary inhomogeneous concentration structures like spots and stripes, breaking the symmetry of the feeding boundary, can spontaneously emerge due to a Turing instability.[6−10]

The CDI reaction, which contains no malonic acid, can be considered as a minimum bistable and oscillatory system in the CI family. In contrast to the previously mentioned reactions, the CDI only exhibits "clock" dynamics in batch conditions, that is, a rapid jump to a state close to equilibrium after an induction time characterized by a low reaction rate. The most detailed model of the CDI reaction is the eight-variable model of ref 2. It accounts for the reversibility of some reaction steps which, compared to simpler models, avoids the iodide concentration falling to unrealistic low values. When the CDI reaction is operated in an open gel reactor, it gives rise to spatial bistability (i.e., two different stationary concentration profiles are stable for the same stationary composition of the CSTR (see section 2)). The difference between states may be revealed by the contrast in color densities due to the presence of an iodine color indicator in the gel (starch or PVA). Thus, the relative stability of these two stationary stable states can be checked by following the direction of motion of the chemical fronts connecting these two states in a same reactor with uniform spatial constraints. A discussion of the generic mechanism of spatial bistability and its experimental evidence in the CDI reaction are presented in refs 13 and 14.

The recent experimental studies of Szalai and De Kepper[1] had two purposes: First, these authors investigated the capability for reactions of the CI family to display stable stationary concentration patterns resulting from front interactions within the domain of the control parameter corresponding to spatial bistability. They also searched for some connection of these hypothetical stationary inhomogeneous structures with those arising from the classical Turing mechanism. To this end, they used the following input species in the CSTR: ClO_2, I^-, I_2, MA, and PVA, and operated under constant midly acid conditions. In addition to the role of color indicator, PVA creates complexes with iodides that are practically immobilized in the gel. This property is essential in experiments on stationary pattern formation.[10,16−18] Complexation also modifies the effective kinetics, which increases the domain of bistability at the expense of the oscillatory domain.[14] The concentrations of MA and I^- in the total input flow, respectively $[MA]_0$ and $[I^-]_0$, were selected as the expandable control parameters. This particular choice has the attractive feature that the well-known behavior of the CDIMA reaction is exactly recovered as $[I^-]_0 \rightarrow 0$. Besides, on the axis $[MA]_0 = 0$, the system is close to the

10.1021/jp046138b CCC: $30.25
Published on Web 01/28/2005

standard CDI reaction studied in ref 14, except that I_2 is not only produced in the reactor but also present in the input flow.

Our aim in this paper is to frame these experiments within a detailed model combining the rate laws that are known to correctly describe the chemistry in the two limiting cases of the CDI and the CDIMA systems. As we will show, the addition of one equation to the CDI model to account for the reaction between I_2 and MA is sufficient to closely capture the dynamical behavior observed in real experiments.

This paper is organized as follows: In section 2, we briefly review the modeling of the experimental setup and its mathematical representation. We also shortly summarize the mechanism of spatial bistability and some features of the CDI reaction that are useful to interpret the results. Section 3 introduces the simple extension to the model of the CDI that we analyze in this paper to account for the experiments, as well as the method and control parameter values used for the integration. In section 4, we report the numerical results and compare them with the experimental ones. The complete set of rate equations as well as the kinetic constants and equilibrium parameters used in the simulations are gathered in the Appendix. The last section is devoted to our conclusions and opening for future work.

2. Background

In this paper, we consider the set of experiments of ref 1 that were performed in a one-sided fed reactor with an annular geometry. In this type of reactor, a flat ring of gel that can be described as a thin circular band is fed by the CSTR along the outer radius, while the inner radius R of the gel is kept in contact with an impermeable wall. The dimensions of the gel are such that both radii of curvature are much larger than the difference between them, hereafter referred to as the "depth", and denoted by d. Because the thickness of this flat ring is also smaller than the depth, one can regard the system as two-dimensional, and consider the feeding boundary to be a line. Thus, in the mathematical description, we keep only the orthogonal and tangential directions to the circular feeding boundary. While the phenomenon of spatial bistability is observed along the radial direction, the Turing bifurcation breaks the symmetry along the tangential direction. Because $R \gg d$, we can neglect the effect of curvature in the simulations and consider the gel as a rectangular sheet with periodic boundary conditions in the direction parallel to the feeding edge.

The numerical simulations assume that the coupled dynamical equations for the concentrations in the CSTR and in the gel are respectively given by[14]

$$\frac{\partial c_{i\mathrm{h}}}{\partial t} = f_i(\mathbf{c}_\mathrm{h}) + \frac{(c_{i0} - c_{i\mathrm{h}})}{\tau} + G_i \tag{1}$$

and

$$\frac{\partial c_i}{\partial t} = f_i(\mathbf{c}) + D_i \nabla^2 c_i \tag{2}$$

where τ denotes the residence time in the CSTR; c_{i0}, $c_{i\mathrm{h}}$, and c_i are the concentrations of species i, respectively, in the input flow, in the CSTR, and inside the gel; D_i is the corresponding diffusion coefficient; and the f_i's are the reaction rates. In the right-hand side of eq 1, the three terms represent the changes of the concentrations per time unit. The first term gives the contribution of the reactions. The second one represents the input and output flows of the species. It contains all the expandable control parameters of the system, namely, τ and the c_{i0}. The third one represents the feedback of the gel contents on the CSTR and is proportional to the diffusion flow of the species through the surface of contact, S. Thus

$$G_i \propto \frac{1}{V} D_i \int_S \nabla c_i \cdot \mathbf{n}\, \mathrm{d}S \tag{3}$$

where V is the volume of the CSTR and $\mathbf{n}$ is the unit vector orthogonal to the boundary. The strength of this term then depends on the concentration profile inside the gel and, for a constant section, on the ratio of volumes of the CSTR and the gel. Even if the feedback effect can be reduced by making the volume of the CSTR larger, we decided to keep the real ratio of volumes and include this feedback in the simulations, except otherwise stated. It turns out that, under real experimental conditions, the drag on the CSTR contents due to this term can be noticeable (the shifts induced in the transition points are larger than the typical resolution), except for profiles that are almost flat at the boundary (i.e. when $[\nabla c_i]_S \approx 0$).

In the mathematical representation of the annular reactor, proper boundary conditions are periodic in the direction parallel to the feeding edge and zero flux at the impermeable wall. If the CSTR state can be computed independently of the gel (i.e., when $G_i = 0$), when solving eq 2, the CSTR state obtained from eq 1 defines Dirichlet boundary conditions on the gel−CSTR interface. However, because of the presence of the feedback, the boundary conditions will have to be constantly updated in the course of the evolution to correct the concentrations in the CSTR.

Central to this paper is the phenomenon of spatial bistability that we shortly review here. Spatial bistability is usually related with autocatalytic chemical reactions that display clock behavior in closed systems. In batch conditions, such behavior is easily recognized by the existence of an induction time τ_{ind} characterized by a low reaction rate, followed by a sharp acceleration period in which the reaction is ignited and the system essentially switches to a state which is close to the asymptotic state of thermodynamic equilibrium. In a CSTR, such a reaction will display bistability (hysteresis) between an unreacted (or flow, F) and a reacted (or thermodynamic, T) stationary state, which is respectively observed for small and large τ's compared with the τ_{ind}. We denominated the reacted state *thermodynamic* because the limit case of a closed system ($\tau \rightarrow \infty$), where the sole stationary state is that of thermodynamic equilibrium, belongs to the same branch as T. In experiments where τ is fixed, the hysteresis between both states can also be obtained, changing τ_{ind}. This can be acomplished by changing the input flow of some species that control the activatory process.

Spatial bistability in the gel in contact with the CSTR can be understood in similar terms as was the "temporal" bistability. The two time scales that are relevant here are τ_{ind} and τ_{dif}, the latter being the characteristic time in which fresh reactants are transported by diffusion from the CSTR to a given point inside the gel. This time depends on the position, as the square of the distance to the CSTR boundary. The simplest way to visualize the phenomenon of spatial bistability is to consider that the depth d of the gel can be varied, and that the contents of the CSTR are kept in the F state. If the gel is thin enough so that $\tau_{\mathrm{ind}} > \tau_{\mathrm{dif}}$, then, even in those points more apart from the feeding boundary, the state of the chemical reaction will be close to that of the CSTR. In other words, at small distances, diffusion is fast enough compared to the reactions so as to keep all the gel in essentially the same flow state as that of the contents of the CSTR (F profile). If d is increased, there will be a critical value where the amount of fresh reactants that are exchanged by diffusion with the CSTR will be insufficient to keep the flow

state close to the impermeable wall where $\tau_{ind} < \tau_{dif}$. Then, the extent of the reaction will be large in those regions, which will be in the T state. The state of the gel, where the composition abruptly changes from the branch F to T somewhere along the depth, is called the mixed state (M profile), and represents a chemical front. Across the front, the concentration of some species usually vary by several orders of magnitude over a short distance. The corresponding spatial behavior to the hysteresis loop discussed above is observed for an intermediate range of *d*: two different spatial distribution of chemicals (the F and M profiles) can be stable for the same F state of the CSTR and exhibit hysteresis as a function of some of the control parameters. Note that spatial bistability can also be obtained for a fixed *d* within a range of other CSTR control parameters. As we will see, when the CSTR is bistable, not only these two profiles can coexist for the same values of the controls, but also a third one, where the CSTR is in the T state (T profile).

The existence of overlapping domains of stability between two different states in the gel for the same state of the CSTR admits the generation of a chemical front connecting those states. This can be accomplished by appropriate initialization of the system, where contiguous sections of the gel are prepared with each state. The relative stability can be asserted by looking at the direction of motion of the interface between them. The direction of propagation can be reversed by varying the control parameters. Not only are the reaction and diffusion processes relevant to determining the motion, but also is the curvature of the interface, which is in part ruled by the thickness of the system. The thinner is the gel, the stronger is the influence of the boundary condition, so that the state of the CSTR (either the F or the T) becomes more favored.

To establish the link with the particular case of the CDI bistable reaction, we mention that in the key reaction step, I_2 is produced autocatalytically in a reaction inhibited by the substrate I^-. Thus, it is expected that a domain of spatial bistability will be obtained along the $[I^-]_0$ axis. As mentioned above, we will consider $[MA]_0$ to be the other bifurcation parameter. In section 4, we will show that, indeed, malonic acid provides the additional feedback mechanism that decreases the CSTR bistability range. In fact, when $[MA]_0$ is increased, an extra source of I^- at the expense of I_2 is introduced, favoring the F state, and thus collapsing the domain of bistability toward smaller values of $[I^-]_0$. By further increasing $[MA]_0$, the bistability eventually disappears in a crossing point, giving rise to oscillations.

3. The Model

The simplest extension to the model of ref 2 for the CDI system, which takes into account the presence of MA and PVA, is to add the following reactions:

$$MA + I_2 \rightarrow IMA + I^- + H^+$$

$$S + I_2 + I^- \underset{k_{s-}}{\overset{k_{s+}}{\rightleftharpoons}} SI_3^- \qquad (4)$$

The empirical rate law of the first equation is well-known, as well as the parameters at normal temperature (see Appendix and ref 12). The second equation accounts for the formation of the PVA−triiodide (SI_3^-) complex. The comparisons of the simulations with the experimental results are good enough to neglect other reactions that are certainly induced by the presence of MA. The system of rate equations that define f_i terms of eqs 1 and 2, as well as the parameters used, are given in the Appendix.

TABLE 1: pH-Dependent Constants

$K_{2H} = k_{2a}/[H^+] + k_{2b}$
$K_{-2H} = k_{-2a}K_{H_2OI^+}/(K_{H_2OI^+} + [H^+]) + k_{-2b}[H^+]/(K_{H_2OI^+} + [H^+])$
$K_{3H} = k_3[H^+]/(K_{HClO_2} + [H^+])$
$K_{4H} = k_4[H^+]/(K_{HClO_2} + [H^+])] \times [K_{H_2OI^+}/(K_{H_2OI^+} + [H^+])]$
$K_{5H} = k_5[H^+]/(K_{HClO_2} + [H^+])$
$K_{8H} = k_8[H^+]$
$K_{-8H} = k_{-8}[K_{H_2OI^+} + [H^+])]^2$
$K_{10H} = k_{10}[H^+]/(K_{H_2OI^+} + [H^+])$

TABLE 2: Kinetic Constants

$K_{HClO_2} = 2 \times 10^{-2}$ M	$k_5 = 10^6$ M^{-1} s^{-1}
$K_{H_2OI} = 3.4 \times 10^{-2}$ M	$k_6 = 4.3 \times 10^8$ M^{-1} s^{-1}
$k_1 = 6 \times 10^3$ M^{-1} s^{-1}	$k_7 = 1.5 \times 10^3$ M^{-1} s^{-1}
$k_{2a} = 1.98 \times 10^{-3}$ M s^{-1}	$k_8 - 10^9$ M^{-2} s^{-1}
$k_{-2a} = 3.67 \times 10^9$ M^{-1} s^{-1}	$k_{-8} = 22$ M^{-1} s^{-1}
$k_{2b} = 5.52 \times 10^{-2}$ M^{-1} s^{-1}	$k_9 = 25$ M^{-1} s^{-1}
$k_{-2b} = 3.48 \times 10^{-2}$ M^{-1} s^{-1}	$k_{10} =$ M^{-1} s^{-1}
$k_3 = 7.8$ M^{-1} s^{-1}	$k_{s+} = 1 \times 10^8$ M^{-2} s^{-1}
$k_4 = 6.9 \times 10^7$ M^{-1} s^{-1}	k_{s-} 1 s^{-1}
$k_{11} = 2.0 \times 10^1$ M^{-1} s^{-1}	$k_{12} = 1.0 \times 10^4$ M^{-1}

The construction of the nonequilibrium phase diagram is mainly performed in 1-D, keeping the direction orthogonal to the CSTR boundary, because except for the study of Turing patterns and fronts, where the natural symmetry is broken, the other direction is irrelevant from the dynamical point of view. In 1-D, the reaction−diffusion equations are integrated by the standard method of lines. The time integrator is the Deufhlard semi-implicit midpoint method for stiff systems.[19] When 2-D computations were necessary, we made use of the code developed by Hindmarsh et al.[20] for stiff systems. In all our numerical experiments, we fixed the residence time to $\tau = 500$ s in agreement with the experimental value. The depth of the gel is 0.5 mm. In the 2-D simulations, the size in the transverse direction was 1.3 mm for the study of Turing structures and 2.0 mm for the case of fronts. The concentrations of the species that are kept at a constant nonzero flow have, according to the experiments, the following input values: $[I_2]_0 = 1.2$ mM, $[ClO_2]_0 = 0.2$ mM. The total concentration of PVA is maintained at 10 g/L, a value that was large enough to supress oscillations in the CSTR in the CDIMA limit and that allowed for the emergence of a Turing structure. Given that many of the parameters are not available in the literature at the temperature in which the experiments were performed (4 °C), we decided to use the complete set only available at 25 °C (see Tables 1 and 2). In this way, we do not aim for a quantitative assessment of the experimental results, but for a test of the qualitative features of the model using parameters that are fully consistent with previous measurements.

In the next section, we summarize the results obtained by the integration of eqs 1 and 2 with reactions terms given by eq 5 and the boundary conditions already discussed.

4. Results

4.1. Phase Diagram in the CSTR. As in the experiments, the CSTR phase diagram exhibits the standard cross-shaped features observed for many other bistable reactions.[11] When $[MA]_0 = 0$ (the CDI reaction limit), the feed composition is similar to that used for the studies in ref 14. The only difference is the presence of I_2 in the flow. We found in our calculations that even small amounts of I_2 ($[I_2]_0 \approx 10^{-3}$ mM) are enough to suppress the CSTR oscillations previously observed. Nevertheless, the essential properties of the CDI reaction, that is, "clock-dynamics" in batch and steady-state bistability in the CSTR, are preserved. Because in the CDI system I_2 is produced autocatalytically in a reaction inhibited by the substrate I^-, the

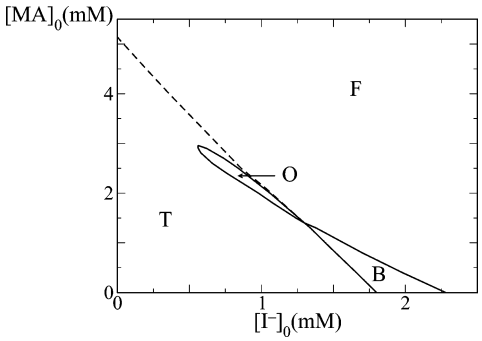

Figure 1. CSTR nonequilibrium phase diagram of the extended model. T, thermodynamic branch; F. flow branch; B, bistability domain; O, oscillatory domain. See text for an explanation of the dashed line.

system is on a T branch at small $[I^-]_0$ and on an F branch at large $[I^-]_0$. Transition between branches occurs with hysteresis at intermediate concentrations. Increasing $[MA]_0$ introduces an additional source of I^- at the expense of I_2. This source favors the F state, which moves the region of bistability to smaller values of $[I^-]_0$, as shown in Figure 1. On further increasing $[MA]_0$, the bistability domain eventually terminates at a cross point, and gives way to a domain of oscillations. This domain, interposed between the continuation of the T state for lower values of $[I^-]_0$ and that of the F state for higher $[I^-]_0$, eventually disappears for higher $[MA]_0$. Beyond that, a branch smoothly connecting the states coming from the T and F is then left. To be consistent with the definition proposed in ref 1, for $[MA]_0$ above the crossing point, we denominate T (F) those states that are to the left (right) of the dashed line in Figure 1. This line joins the inflection points of the curves of stationary concentration values of $[I^-]$ as a function of $[I^-]_0$, obtained for different values of $[MA]_0$. When $[MA]_0 = 5.14$ mM, the production of $[I^-]$ by reaction 4 is so large that the F state extends down to $[I^-]_0 = 0$. Along the $[I^-]_0 = 0$ axis, the situation corresponds exactly to the CDIMA system. The same behavior previously observed in experiments[1,10,15] was obtained numerically: two well-differentiated stationary states for low and high $[MA]_0$ (corresponding respectively to the T and F states) are connected smoothly without oscillations, thanks to the presence of PVA in large-enough concentration.

The small amplitude oscillations that were observed experimentally in a narrow domain of $[I^-]_0$ even at $[MA]_0 = 0$ in the CSTR, but not within the gel, were not found in the computations.

4.2. Phase Diagram in the Gel. In Figure 2, we show the computed nonequilibrium phase diagram of space states in the gel, obtained with the extended kinetic model. Let us first analyze the behavior for low values of $[MA]_0$ (below the crossing point in the CSTR) when no major departures from the pure CDI are expected. Figure 3 shows a typical $[I^-]$ profile in the region denoted by T in Figure 2. The fact that in the CSTR reactants are not truly exhausted is noticeable here by the departure from the flat profile that would be obtained if the contents of the CSTR were in the asymptotic state of thermodynamic equilibrium, a situation where just the diffusion of final products takes place. Inside the T/M/F domain, three types of profiles coexist for the same constraints (Figure 4). One of them is the T profile, obtained by increasing $[I^-]_0$ from the T region. The other two profiles, M and F, correspond to spatial bistability with contents of the CSTR in the F state. Above the T/M/F-to-M/F boundary, the contents of the CSTR can be only in the F state, and just the M/F spatial bistability remains. For still higher values of $[I^-]_0$, the induction time becomes large

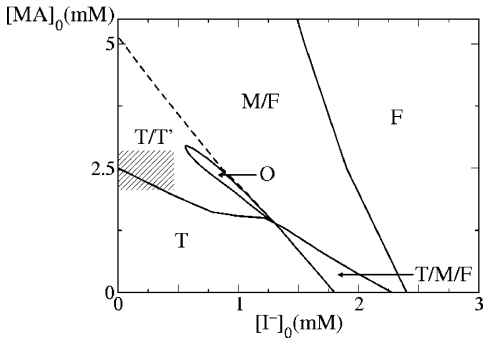

Figure 2. Nonequilibrium phase diagram of the extended kinetic model in the gel. T and T/T′, respectively, the monostable and spatial bistability domain in the gel with the CSTR in the T state; F and M/F, idem, with the CSTR in the F state; T/M/F, domain of coexistence of three stationary profiles (T, M, and F), when the CSTR is bistable; O, domain of oscillations in the gel. The T/T′ spatial bistability region partially overlaps with the Turing domain. Turing spots were observed inside the hatched area. Above $[MA]_0 = 37.2$ mM, only the F profile can be established in the gel (not shown).

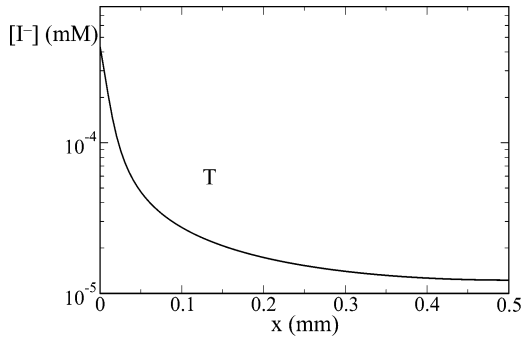

Figure 3. Stationary profile in the depth of the gel in the monostable T region: $[I^-]_0 = 1$ mM, $[MA]_0 = 0$. The CSTR is located at the origin.

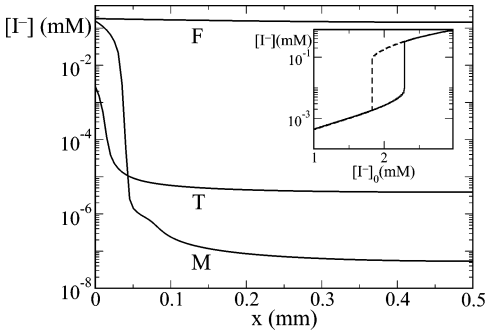

Figure 4. F, T, and M stationary profiles in the depth of the gel for $[I^-]_0 = 2$ mM and $[MA]_0 = 0$. The insert shows the hysteresis loop in the CSTR: the solid (dashed) line is the sequence of stationary states increasing (decreasing) $[I^-]_0$.

compared with the diffusion time even in those regions most apart from the feeding boundary, so that the F profile becomes the only stable one. With increasing $[MA]_0$, the three-state region collapses at the CSTR crossing point, where oscillations also appear in the gel. Interestingly, as observed in the experiments, the spatial bistability region enlarges as $[MA]_0$ is increased, and it is possible to find M/F spatial bistability even far from the parameter region where the CSTR exhibits bistability. Monostability in the CSTR does not preclude the reaction from being bistable under the different conditions that are attained inside the gel.

Furthermore, when $[MA]_0$ is increased above the crossing point, another set of spatial bistable states is observed for low values of $[I^-]_0$, when the CSTR contents belongs to the

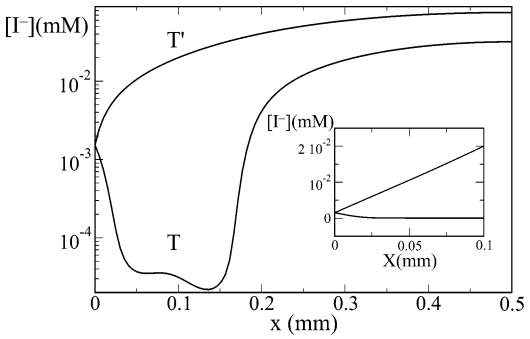

Figure 5. Spatial bistability in the continuation of the thermodynamic branch. Stationary concentration profile of $[I^-]$ in the depth of the gel. Control parameters: $[MA]_0 = 2.7$ mM and $[I^-] = 0$ M. The insert focuses on the region of the gel closest to the CSTR, in linear scale.

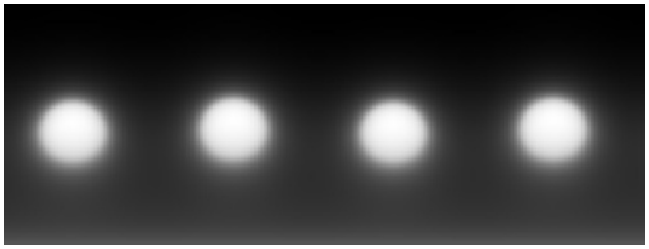

Figure 6. Monolayer of Turing spots in the nine-variable model. $[I^-]$ map: full gray scale (maximum black, minimum white). Control parameters: $[MA]_0 = 2.4$ mM, $[I^-]_0 = 0.1$ mM. Gel size 0.5×1.35 mm. CSTR connected at the bottom line. Impermeable wall at top.

continuation of the thermodynamic branch (the T/T′ domain in Figure 2). The T′ profile (Figure 5) is obtained from the F profile, by decreasing $[MA]_0$ from a state above the dashed line. Multiple solutions coexisting while the CSTR is in the T state may seem paradoxical at first glance. However, note that by adding MA the reaction dynamics becomes more involved, with an in situ slow source of I^- for a given $[I^-]_0$ and residence time. We have indeed moved away from a situation of genuine thermodynamic equilibrium that is only achievable in the limit where all the fluxes are zero and after long-enough time. Thus, at high enough $[MA]_0$, multiplicity of solutions is not forbidden. Again, note that the T state of the CSTR is not a true equilibrium state (as can be seen from Figures 3 and 4, the I^- ion concentration drops by 2 orders of magnitude in the gel). As before, this new domain of spatial bistability T/T′ can exist even if the CSTR is monostable. Experimentally, spatial bistability was only observed with the CSTR in the F state.

As in the experiments, a monolayer of Turing spots (Figure 6) is observed in 2-D simulations within the hatched zone of the phase diagram. The Turing domain already observed in the "pure" CDIMA reaction ($[I^-]_0 = 0$) extends for values up to $[I^-]_0 \approx 0.5$ mM. As seen in Figure 2, the domain where we find spots in the numerical simulations partially overlaps with the new region of spatial bistability: If the gel is initially prepared everywhere with the T profile obtained in the 1-D simulations (Figure 5), it becomes unstable to diffusion in the orthogonal direction. In other words, in 2-D, the system undergoes an instability that breaks the symmetry of the initial condition, which is invariant under translations parallel to the feeding boundary. On the contrary, the T′ state remains stable in 2-D. The wavelength of the pattern, which varies from 0.25 to 0.35 mm within the hatched domain, is in good agreement with those typically measured in the experiments. Interestingly, by slightly varying some of the parameters, two rows of spots could also be obtained (Figure 7).

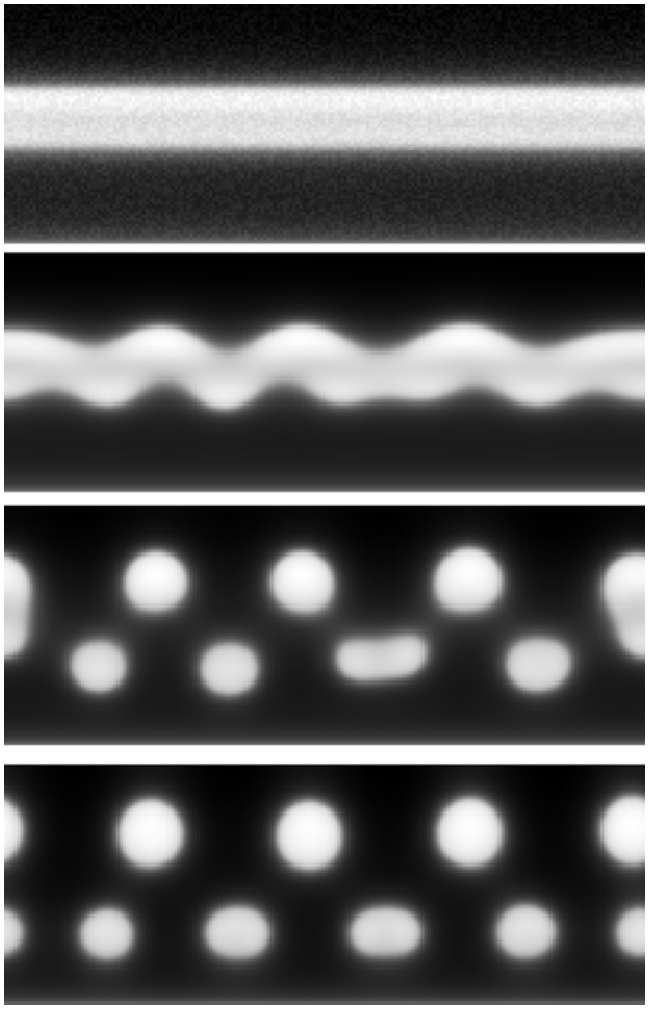

Figure 7. Time evolution of $[I^-]$ starting from a 1-D stationary profile with a random perturbation. From top to bottom, $t = 0$ s, $t = 500$ s, $t = 1000$ s, $t = 2500$ s. Conditions are slightly different compared to the experiments. Control parameters: $\tau = 50$ s, $[I_2]_0 = 1.0$ mM, $[ClO_2]_0 = 0.2$ mM, $[I^-]_0 = 0$ M, $[MA]_0 = 0.7$ mM.

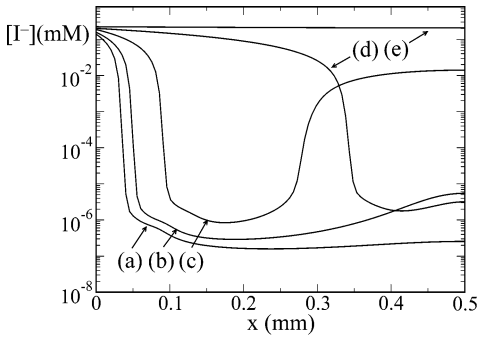

Figure 8. Stationary concentration profiles for $[I^-]_0 = 1.5$ mM and (a) $[MA]_0 = 3.0$ mM; (b) $[MA]_0 = 3.5$ mM; (c) $[MA]_0 = 4.5$ mM; (d) $[MA]_0 = 5.0$ mM; (e) $[MA]_0 = 6.0$ mM. The figure shows the recovery effect close to the impermeable wall due to the input flow of MA, and the transition from the mixed M state to the spatially uniform flow state as $[MA]_0$ is increased.

In Figure 8, we present the stationary profiles of $[I^-]$ obtained by fixing $[I^-]_0 = 1.5$ mM and increasing $[MA]_0$. This figure highlights the effect of reaction 4 on the stationary profiles. While for $[MA]_0 = 3.0$ mM, there is no significant recovery of $[I^-]$, for $[MA]_0 = 4.5$ mM, the increase of $[I^-]$ close to the impermeable wall is large. Because low (high) $[I^-]$ looks white (black) in the experiments, a bright region inside two dark ones

is observed in the gel, parallel to the CSTR, when the recovery is large enough. As we shall see in section 4.3, front repulsion is facilitated in this case. For higher $[MA]_0$, the transition from the mixed M profile to the roughly spatially uniform F one is achieved.

Finally, we mention that, when $[MA]_0 > 37.2$ mM, the spatial bistability completely disappears as a function of $[I^-]_0$, and only the F profile can be established in the system. Even if we lack experimental data to check this result, the tendency observed in the experiments is similar (i.e., a uniform F profile becomes favored for high $[MA]_0$).

4.3. Front Interactions. In the study of fronts, we restrict our investigation to the experimental conditions, and analyze only those fronts that are possible when the CSTR is in the F state. The system was initially prepared with an M profile in some portion to the left (usually one-half the length of the gel) and the F profile in the rest. In general, after a transient, a fixed profile moving rigidly to either side should be established, with the direction of motion depending on the values of $[I^-]_0$ and $[MA]_0$. Because the feedback term depends on the size of the variable proportion of gel within the states F or M (a situation that would have no meaning if the ideal situation of an infinite system were possible), we set a Dirichlet boundary condition in the CSTR boundary, and thus neglect the influence of the (otherwise variable) feedback term in the equations. This simplifying assumption is a posteriori well-justified, because the transition boundary between M/F and F does not significantly deviate from the boundary determined when the feedback was accounted for. Moreover, in accordance with the experiments, stationary inhomogeneous structures due to front repulsion were found close to this limit. Given that our aim here was the study of front−front interactions, we also changed the periodic boundary condition into zero flux. Thus, we examine the interaction of a front with its mirror image and make the additional underlying assumption that solutions (fronts) do not break the symmetry with respect to these boundaries.

In agreement with the experiments, we find that in the M/F spatial bistability domain, the mixed state finally settles in the whole gel, except for a thin region of parameters close to the boundary between M/F and F. In other words, the domain where the front velocity is reversed is close to this transition limit. If a repulsive mechanism is able to stabilize front pairs, creating inhomogeneous stationary structures, these should be observed, at least close to this "zero velocity" range, where fronts move slowly. To this end, we made a series of numerical experiments, keeping the same value of $[I^-]_0 = 1.2$ mM in the CSTR and varying $[MA]_0$, in a region where all the fronts move slowly to the right (i.e., M is more stable). The initial condition was prepared as in the top image of Figure 9. As the front advances to the right, it starts to "feel" the interaction with its "mirror" image. The presence of repulsion can be noted by the velocity decrease. When $[MA]_0$ was such that the M profile looked like (a) or (b) in Figure 8, the repulsion was insufficient to halt the fronts. They eventually ended by merging with their mirror images. Again, in complete agreement with the experimental results, only when the recovery is noticeable (like in the (c) profile of Figure 8) and the mixed profile is visualized by a clear bright stripe, as in Figure 9, the front approaches a stable equilibrium position at 0.8 mm of its mirror image close to the 0.7 mm measured in the experiments (see Figure 10). The stability of this asymptotic state was established by rigidly shifting the front to the right or left in the neighborhood of such a point (i.e., toward or away from the right boundary, respectively) and checking that the system returns to the same position.

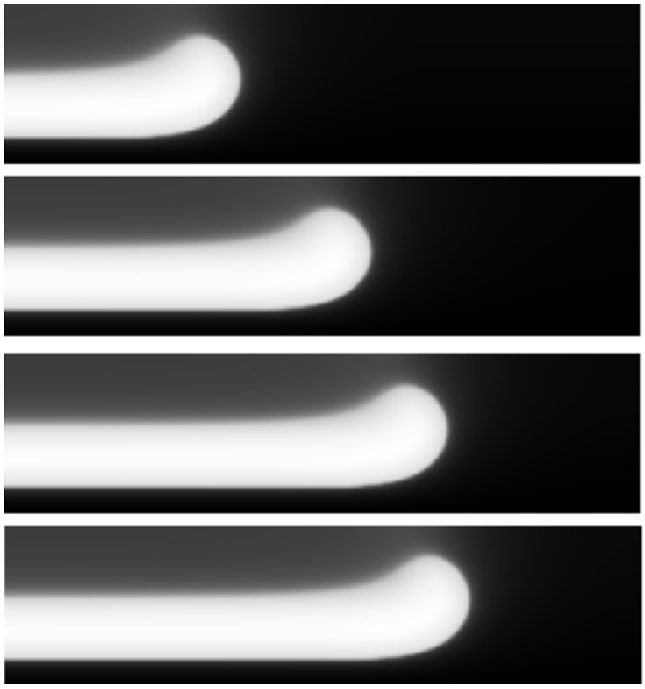

Figure 9. Motion of the M/F interface: distribution of $[I^-]$ at consecutive frames (time interval 2×10^4 s, evolution from top to bottom). Full gray scale: maximum black, minimum white. Control parameters: $[I^-]_0 = 1.2$ mM, $[MA]_0 = 7.6$ mM.

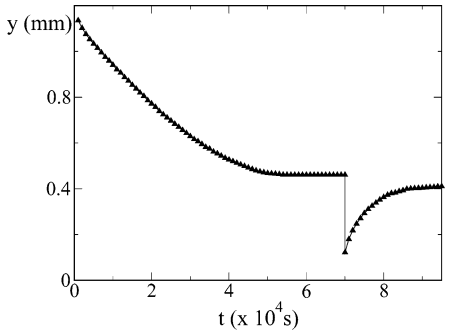

Figure 10. Time evolution of the position of the tip of the front. The position is measured from the right border of the gel. At time $t = 7 \times 10^4$, the front was rigidly shifted to the right. Same parameters as in Figure 9.

5. Discussion and Conclusions

In this paper, we have shown that the sole addition of eq 4 to the CDI model of ref 2 is enough to capture all the qualitative aspects of the real experiments on the CI-driven system studied in ref 1. An exact quantitative comparison was outside the possible scope because of the lack of data in the literature with respect to the parameter values at the temperature at which the experiments were carried out.

Among the new dynamical behavior of the CI family, stationary and stable inhomogeneous structures maintained by front−front interactions were observed, in remarkable correspondence with the experiments. This behavior is not seen in the CDI reaction, probably because in the presence of PVA, the diffusive transport of I^- ions from the CSTR boundary is slower than of the ClO_2^-. This introduces a deficiency of I^- at the innermost part of the gel that lateral diffusion through the front cannot compensate. The introduction of MA makes up for this deficit through reaction 4, which facilitates the lateral front repulsion.

Closely following experimental findings, we obtained spatial bistability, front interactions, and Turing patterns in similar regions of the phase diagram. In addition, even noticeable characteristics such as the large extension of the spatial bistability region compared to the one of temporal bistability of the CSTR were captured. It is indeed possible to find spatial bistability even far from the parameter region where the CSTR exhibits bistability. Monostability in the CSTR does not prevent spatial bistability in the gel.

In contrast to the experiments, we have found that the phenomenon of spatial bistability is not restricted to a region of parameters where the CSTR contents belong to the flow branch, but a new domain of bistability with the CSTR in the continuation of the T branch can also be observed. Even more interestingly, this region can coexist with the one where Turing patterns appear. This coexistence has also been recently sustained in calculations on model equations such as the Gray−Scott model.[21] However, even in this comparatively simple case, it is unclear if this overlapping implies a close relation between both phenomena. It would be interesting to proceed with the investigations along this lines, because while the phenomenon of the Turing instability has been, up to now, rare in real chemical reactions, spatial bistability is expected to be a more generic phenomena in autocatalytic reactions. The results that we report here correspond only to the fronts observed in the experiments connecting the F with the M states. More complete studies of these fronts characterizing asymptotic velocities as a function of controls and basins of attraction, as well as for those fronts that are possible in the new region of spatial bistability (with the CSTR in the T state), are the subject of a work in progress.

Acknowledgment. We wish to acknowledge useful discussions with I. Szalai. D.E.S. thanks the Ministry of Education of France for financial support.

Appendix

The rate equations that define the extended model are given by

$$\mathrm{d}[\mathrm{ClO_2^-}]_{tot}/\mathrm{d}t = k_1[\mathrm{I^-}][\mathrm{ClO_2}] - (K_{3H}[\mathrm{I^-}] + K_{4H}[\mathrm{HOI}]_{tot} + K_{5H}[\mathrm{HIO_2}])[\mathrm{ClO_2^-}]_{tot}$$

$$\mathrm{d}[\mathrm{I^-}]/\mathrm{d}t = -k_1[\mathrm{I^-}][\mathrm{ClO_2}] + K_{2H}[\mathrm{I_2}] - K_{-2H}[\mathrm{I^-}][\mathrm{HOI}]_{tot} - K_{3H}[\mathrm{ClO_2^-}]_{tot}[\mathrm{I^-}] - k_6[\mathrm{I^-}][\mathrm{HOCl}] - K_{8H}[\mathrm{I^-}][\mathrm{HIO_2}] + K_{-8H}[\mathrm{HOI}]_{tot}^2 + K_{10H}[\mathrm{HOI}]_{tot}[\mathrm{HIO_2}] - k_{s+}[\mathrm{S}][\mathrm{I^-}][\mathrm{I_2}] + k_{s-}[\mathrm{SI_3^-}] + \frac{k_{11}[\mathrm{MA}][\mathrm{I_2}]}{1 + k_{12}[\mathrm{I_2}]}$$

$$\mathrm{d}[\mathrm{HOCl}]/\mathrm{d}t = (K_{3H}[\mathrm{I^-}] + K_{4H}[\mathrm{HOI}]_{tot} + K_{5H}[\mathrm{HIO_2}])[\mathrm{ClO_2^-}]_{tot} - k_6[\mathrm{I^-}][\mathrm{HOCl}] - k_7[\mathrm{HOCl}][\mathrm{HIO_2}]$$

$$\mathrm{d}[\mathrm{HOI}]_{tot}/\mathrm{d}t = K_{2H}[\mathrm{I_2}] - K_{-2H}[\mathrm{I^-}][\mathrm{HOI}]_{tot} + (K_{3H}[\mathrm{I^-}] - K_{4H}[\mathrm{HOI}]_{tot})[\mathrm{ClO_2^-}]_{tot} + k_6[\mathrm{I^-}][\mathrm{HOCl}] + 2K_{8H}[\mathrm{I^-}][\mathrm{HIO_2}] - 2K_{-8H}[\mathrm{HOI}]_{tot}^2 + k_9[\mathrm{HIO_2}]^2 - K_{10H}[\mathrm{HOI}]_{tot}[\mathrm{HIO_2}] \quad (5)$$

$$\mathrm{d}[\mathrm{I_2}]/\mathrm{d}t = k_1[\mathrm{I^-}][\mathrm{ClO_2}]/2 - K_{2H}[\mathrm{I_2}] + K_{-2H}[\mathrm{I^-}][\mathrm{HOI}]_{tot} - k_{s+}[\mathrm{S}][\mathrm{I^-}][\mathrm{I_2}] + k_{s-}[\mathrm{SI_3^-}] - \frac{k_{11}[\mathrm{MA}][\mathrm{I_2}]}{1 + k_{12}[\mathrm{I_2}]}$$

$$\mathrm{d}[\mathrm{HIO_2}]/\mathrm{d}t = (K_{4H}[\mathrm{HOI}]_{tot} - K_{5H}[\mathrm{HIO_2}])[\mathrm{ClO_2^-}]_{tot} - k_7[\mathrm{HOCl}][\mathrm{HIO_2}] - K_{8H}[\mathrm{I^-}][\mathrm{HIO_2}] + K_{-8H}[\mathrm{HOI}]_{tot}^2 - 2k_9[\mathrm{HIO_2}]^2 - K_{10H}[\mathrm{HOI}]_{tot}[\mathrm{HIO_2}]$$

$$\mathrm{d}[\mathrm{ClO_2}]/\mathrm{d}t = -k_1[\mathrm{I^-}][\mathrm{ClO_2}]$$

$$\mathrm{d}[\mathrm{SI_3^-}]/\mathrm{d}t = k_{s+}[\mathrm{I^-}][\mathrm{I_2}][\mathrm{S}] - k_{s-}[\mathrm{SI_3^-}]$$

$$\mathrm{d}[\mathrm{MA}]/\mathrm{d}t = -\frac{k_{11}[\mathrm{MA}][\mathrm{I_2}]}{1 + k_{12}[\mathrm{I_2}]}$$

where $[\mathrm{ClO_2^-}]_{tot} = [\mathrm{ClO_2^-}] + [\mathrm{HClO_2}]$ (total chlorite), $[\mathrm{HOI}]_{tot} = [\mathrm{HOI}] + [\mathrm{H_2OI}]$ (total [HOI]), and $[\mathrm{S}]_0 = [\mathrm{S}] + [\mathrm{SI_3^-}]$, the total concentration of PVA. The values of k_{s+} and k_{s-} are those used by Rudovics et al. to fit experimental data on Turing patterns.[10] The expressions for the pH-dependent constants K_{iH} and the values of the other kinetic constants are gathered in Table 1 and Table 2, respectively. Note that the last terms added in the equations for $[\mathrm{I^-}]$ and $[\mathrm{I_2}]$ in eq 5 represent the consumption rate of [MA].

References and Notes

(1) Szalai, I.; De Kepper, P. *J. Phys. Chem. A* **2004**, *108*, 5315.

(2) Lengyel, I.; Li, J.; Kustin, K.; Epstein, I. R. *J. Am. Chem. Soc.* **1996**, *118*, 3708.

(3) De Kepper, P.; Epstein, I. R.; Kustin, K.; Orbán, M. *J. Phys. Chem.* **1982**, *86*, 170.

(4) De Kepper, P.; Boissonade, J.; Epstein, I. R. *J. Phys. Chem.* **1990**, 6525.

(5) Lengyel, I.; Rábai, G.; Epstein, I. R. *J. Am. Chem. Soc.* **1990**, *112*, 4606; Lengyel, I.; Rábai, G.; Epstein, I. R. *J. Am. Chem. Soc.* **1990**, *112*, 9104.

(6) Turing, A. M. *Philos. Trans. R. Soc. London, Ser. B* **1952**, *237*, 37.

(7) Castets, V.; Dulos, E.; Boissonade, J.; De Kepper, P. *Phys. Rev Lett.* **1990**, *64*, 2953. De Kepper, P.; Castets, V.; Dulos, E.; Boissonade, J. *Physica D* **1991**, *49*, 161.

(8) Ouyang, Q.; Swinney, H. *Nature* **1991**, *352*, 610. Ouyang, Q.; Swinney, H. *Chaos* **1991**, *1*, 411.

(9) Epstein, I. R.; Lengyel, I. *Physica D* **1991**, *84*, 1.

(10) Rudovics, B.; Barillot, E.; Davies, P. W.; Dulos, E.; Boissonade, J.; De Kepper, P. *J. Phys. Chem. A* **1999**, *103*, 1790.

(11) Field, R. J., Burger, M., Eds. *Oscillations and Traveling Waves in Chemical Systems*; Wiley: New York, 1985.

(12) Epstein, I. R.; Pojman, J. A. *An Introduction to Nonlinear Chemical Dynamics*; Oxford University Press: Oxford, 1998.

(13) Blanchedeau, P.; Boissonade, J. *Phys. Rev. Lett.* **1998**, *81*, 5007.

(14) Blanchedeau, P.; Boissonade, J.; De Kepper, P. *Physica D* **2000**, *147*, 283−299.

(15) Davies, P. W.; Blanchedeau, P.; Dulos, E.; De Kepper, P. *J. Phys. Chem. A* **1998**, *102*, 8236.

(16) Lengyel, I.; Epstein, I. *Proc. Natl. Acad. Sci. U.S.A.* **1992**, *89*, 3977.

(17) Pearson, J. E.; Bruno, W. J. *Chaos* **1992**, *2*, 513.

(18) Strier, D. E.; Dawson, S. P. *J. Chem. Phys* **2000**, 112, 2, 825. Strier, D. E.; Dawson, S. P. *Phys. Rev. E* **2004**, *69*, 066207,.

(19) Deuflhard, P. *SIAM Rev.* **1985**, *27*, 505.

(20) Brown, P. N.; Byrne, G. D.; Hindmarsh, A. C. *SIAM J. Sci. Stat. Comput.* **1989**, *10*, 1038−1051.

(21) Benyaich, K.; Borckmans, P. Private communication.